Journal of the European Ceramic Society 41 (2021) 7000–7004

Contents lists available at ScienceDirect

Journal of the European Ceramic Society

journal homepage: www.elsevier.com/locate/jeurceramsoc

Measuring lead scandium tantalate phase transition entropy by infrared camera

Pierre Lhéritier [a], Youri Nouchokgwe [a,b], Veronica Kovacova [a], Chang-Hyo Hong [c], Àlvar Torelló [a,b], Wook Jo [c], Emmanuel Defay [a,*]

[a] Materials Research and Technology Department, Luxembourg Institute of Science and Technology, 41 rue du Brill, Belvaux, L-4422, Luxembourg
[b] Department of Physics and Materials Science, University of Luxembourg, 41 Rue du Brill, Belvaux, L-4422, Luxembourg
[c] School of Materials Science and Engineering, Ulsan National Institute of Science and Technology, Ulsan, 44919, South Korea

ARTICLE INFO

Keywords:
Phase transition
Heat capacity
Ferroelectric
Electrocaloric

ABSTRACT

Using an infrared camera, we measured the latent heat of the first order phase transition in lead scandium tantalate at different applied electric fields. The entropy change value of 3.4 J kg^{-1} K^{-1} is consistent with differential scanning calorimetry measurements. The advantage of such an approach stems from the possibility to obtain both adiabatic temperature change and latent heat of the phase transition material only with an infrared camera or a thermocouple. This may prove useful for a systemic characterization of first order electrocaloric materials.

1. Introduction

With recent advances in the field of caloric materials, new cooling technologies at a reasonable cost seem to be within reach. In order to compete with current vapour compression devices, both prototype architectures and material properties must be improved upon. On the material side, the two main figures of merit are the adiabatic temperature change ΔT and the entropy variation ΔS induced by the application of an external field [1–7]. In electrocalorics, both these quantities become significant near sharp first order transitions. Such transitions can be from ferroelectric to paraelectric ($PbSc_{1/2}Ta_{1/2}O_3$, $BaTiO_3$) [8,9] or antiferroelectric to paraelectric ($Pb_{1-\frac{3}{2}y}La_{2y}Zr_xTi_{1-x}O_3$, $PbZrO_3$) [10,11].

The entropy change is usually estimated from the latent heat of the phase transition using custom-made [12] or commercially available calorimeters. The adiabatic temperature change can be measured with direct techniques such as thermocouples or infrared imaging. Since the two quantities are linked through specific heat, the temperature change can also be inferred from the entropy change and vice-versa [13,14]. However, because of the dependence of the specific heat to temperature and electric field near the phase transition, this is not a fully reliable method.

This paper presents a method of measuring the phase transition entropy change using an apparatus commonly employed to measure the adiabatic temperature change of a caloric material. That way both ΔT and ΔS can be obtained with the same sample, in a single campaign.

The starting idea stems from the use of hysteretic dielectric losses to heat up the sample, induce the phase transition and then extract the latent heat from oddities in the temperature profile as the sample cools down. Using hysteretic losses presents the advantage of having an easily controlled source of heat, dissipated directly into the bulk of the sample. Zheng et al. [15] used this principle to extract the thermal conductivity of a piezoelectric stack of material. More recently Malyshkina et al. [16] showed how specific heat can be measured in ferroelectric materials far away from any phase transition where it can be considered as constant.

We build on these principles to present a new way of measuring the entropy of a first order phase transition. This should be mostly relevant for the study of electrocaloric materials and therefore we applied it to one of its foremost representatives: lead scandium tantalate (PST). This material has recently been used in prominent studies [17,18] in the form of multi layered capacitors which led to record-breaking electrocaloric cooling performances. However, the literature on bulk PST intrinsic performances is still missing. This study is an opportunity to complete the picture.

2. Material and equipment

We mixed oxide powders of PbO (purity 99.9 %), Sc_2O_3 (purity 99.99

* Corresponding author.
E-mail address: emmanuel.defay@list.lu (E. Defay).

https://doi.org/10.1016/j.jeurceramsoc.2021.07.002
Received 22 February 2021; Received in revised form 29 June 2021; Accepted 1 July 2021
Available online 6 July 2021

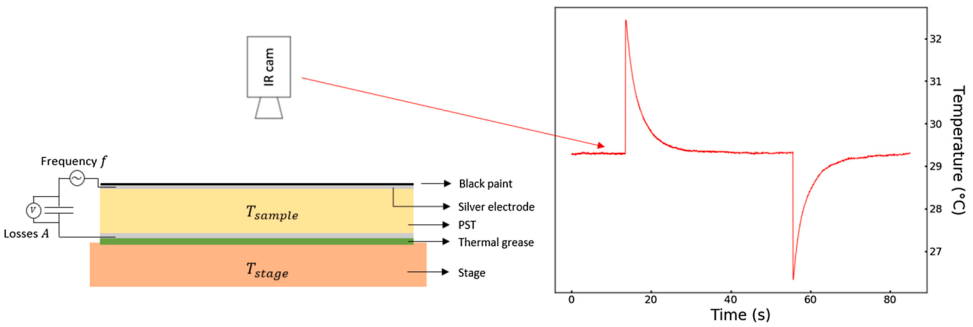

Fig. 1. a: Schematic representation of the experimental setup. Figure b: measured temperature profile of a PST sample at 29.5 °C submitted to a 22 kV cm^{-1} electric field.

%) both from Sigma Aldrich and Ta_2O_3 (purity 99.9 %) from Kojundo Chemical. The respective amounts of these oxides correspond to $PbSc_{1/2}Ta_{1/2}O_3$. A 24 h-ball milling with zirconia has been performed with ethanol. The product powder was calcined at 850 °C for 2 h, crushed and ball-milled another time for 24 h. 30 mm x 10 mm rectangles of PST were pressed up of 180 MPa with addition of polyvinyl alcohol. Sintering was performed in a closed crucible with $PbZrO_3$ and PbO used as sacrificial powders at 1300 °C for 2 h. A final annealing at 1000 °C for 30 h was used to enhance ordering of PST.

The samples exhibit a surface area of 1 cm^2 for a 0.5 mm-thickness. Their degree of order was measured by X-Ray diffraction and reaches 0.96. The samples were electroded with conductive silver paint, which also played the role of glue for connecting wires. A piece of insulating tape (Kapton) was added onto the temperature-controlled stage for electrical insulation and a small amount of thermal grease was spread on it to improve thermal contact. The X-ray diffraction pattern was collected using Bruker D8 diffractometer in reflexion Bragg-Brentano geometry. The 2θ range was set from 15° to 60° with 0.02° step size at 4 s per step. Diffraction peaks have been labelled using the PDF file number 01-074-2635 [19]. The order parameter has been deduced using the ratio of the integrated areas of a collected supercell peak corresponding to the (111) crystallographic plane and unit a cell peak corresponding to the (200) plane. This ratio was compared to a reference ratio of corresponding peaks equal to 1.33 that is associated to an order parameter equal to 1. This number as well as the method are detailed in Wang et al. [20]. Peaks of interest were fitted using a pseudo-Voigt function.

High-resolution micrographs of bulk PST cross-section were obtained using scanning electron microscope (SEM) Helios Nanolab 650 from FEI at a 4 keV acceleration voltage at 4.2 mm working distance. The grain size and pores size was assessed using ImageJ software. Differential scanning calorimetry (DSC) measurements were performed on a METTLER TOLEDO DSC 3+ calorimeter at a speed of 5 K min^{-1}. Temperature was acquired with a FLIR x6580sc infrared camera, calibrated by the manufacturer. Voltage was applied with an Agilent 3390 source meter unit (SMU). The output signal was then amplified by a factor two hundred with a Trek 2220. The sample polarization was measured with a home-made Sawyer-Tower circuit. All electrical signals were acquired using a DSO5014A Agilent oscilloscope. The temperature-controlled stage was a Linkam THMS600 with active cooling (LNP95).

3. Adiabatic temperature change

The first quantity of interest in PST, and electrocaloric materials in general, is the adiabatic temperature change (ΔT_{EC}) obtained when an electric field is applied. As heat is bound to leave the sample, the easiest way to approach adiabaticity is to apply the field as fast as possible and monitor the temperature moments after. This criterion can be met if the time constant of the electric charge is much smaller than the time constant governing the heat exchange. Fig. 1 displays a schematic of the measurement apparatus alongside a typical temperature profile acquired for a ΔT_{EC} measurement.

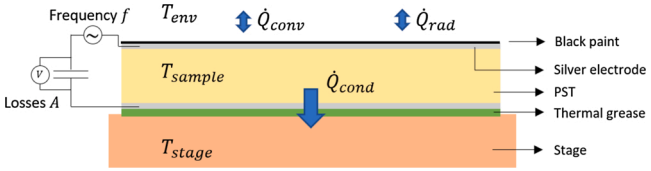

Fig. 2. Schematic of the experiment. The arrows represent the heat flux rates involved in the thermal equations hereafter. The stage is maintained at a temperature below that of the environment. Thus, at any point during the experiment the sample is hotter than the stage and the conductive heat flow rate is pointing toward the plate. The radiative and convective mechanisms can be in either direction throughout the experiment.

The sample is fully electroded and connected to a sourcemeter unit (SMU). It is charged at constant current, using the SMU in current source mode, to reduce breakdown risks. Temperature is monitored all the way by the infrared camera. A typical EC measurement curve is displayed in Fig. 1b. The temperature increases when the electric field is applied, then drops when the electric field is removed. On field removal, the sample cools down and reaches temperature below that of its environment. ΔT_{EC} is considered at its peaking value, meaning 3.0 K in the present example. A full measurement campaign on the EC effect consists of several such measurements, at different voltages and initial temperatures. An example of full characterization of ΔT_{EC} in PST Multi Layer Capacitors (MLCs) with an IR camera can be found in [17]. Here we focus on obtaining ΔS and ΔT simultaneously using IR camera.

4. Phase transition latent heat

We develop first an analytical development to set the experiment, schematically represented in Fig. 2 with the notations of the different physical quantities involved.

Let us consider the energy balance of the sample at the beginning of the experiment, before any electric field is applied. The stage is set at a given temperature T_{stage}, below that of environment T_{env}. The sample temperature T_{sample} is somewhere between T_{env} and T_{stage}, due to the conductive, convective and radiative heat exchanges with the surroundings.

In this initial steady state, there is no net heat flow through the sample boundaries, yielding Eq. 1.

$$\dot{Q}_{conv\_0} + \dot{Q}_{cond\_0} + \dot{Q}_{rad\_0} = 0 \tag{1}$$

$\dot{Q}$ denotes a heat flow rate, the subscripts correspond to the different mechanisms involved (conduction, convection and radiation) and _0 stands for initial steady state. This can be approximated by Eq. 2

$$hS_A\left(T_{sample_0} - T_{env}\right) + \left(T_{sample_0} - T_{stage}\right)\sigma_c S_A + 4S_A\varepsilon\sigma {T_{env}}^3\left(T_{sample_0} - T_{env}\right) = 0 \quad (2)$$

The first term corresponds to the convective heat exchange with the surroundings. The second term is the conductive heat flow between the sample and the stage. h-convective heat transfer coefficient, σ_c -conductive heat transfer coefficient and S_A- sample surface area. The last term is the first order development of the radiative heat exchange. We work near room temperature, so the higher order terms are neglected. ε is sample emissivity and σ is Stephan Boltzmann constant.

When the electric field is applied, the sample energy balance is given by Eq. 3. A heat source term is added, with A the area of the polarization hysteresis and f the signal frequency. As the sample is not in a steady state anymore, the internal energy of the system changes, following Eq. 3.

$$\frac{dU}{dt} = Af + \dot{Q}_{cond} + \dot{Q}_{conv} + \dot{Q}_{rad} \quad (3)$$

Combining Eqs. 2 and 3, the internal energy variation can be expressed as a function of a single temperature difference.

$$\frac{dU}{dt} = Af + \left(\sigma_c S + hS + 4\varepsilon\sigma S {T_{env}}^3\right)\left(T_{sample\ (t)} - T_{sample_0}\right) \quad (4)$$

Or simply

$$\frac{dU}{dt} = Af + \varphi\ \Delta T(t) \quad (5)$$

$\Delta T_{(t)}$ is the temperature of the sample compared to its initial temperature, before the AC signal is applied. φ is a concatenation of the different coefficients because we do not need to discriminate between each contribution. A more detailed development of Eq. 1–5 is presented in supplementary. Eq. 5 applies to any moment in the experiment and we will be interested in the cooling profile, once the electric signal is turned off, meaning when $f = 0$.

The variation of internal energy described by Eq. 5 only involves heat, without any form of work. Strictly speaking, there should be a term for electric work as the sample becomes ferroelectric during cooling, which involves charge displacement in a closed circuit. However, this work only reaches 23 J kg^{-1} at the highest applied DC bias (280 V or 5.6 kV cm^{-1}). As a point of comparison this is the energy needed to heat up the sample by 0.07 °C. Thus, the electric work can be neglected with respect to the heat terms involved.

More than the internal energy variation, the quantity of interest is entropy change. Calculating it requires knowledge on the reversible path taken by the sample to go from one given state to another. So, let us consider a hypothetical path where the sample cools down very slowly, exchanging a small amount of heat δQ_{rev} all the way through the path. The initial and final states are the same in the experimental and hypothetical cases and so is the variation of internal energy ΔU, which gives Eq. 6.

$$\Delta U = \int \delta Q_{rev}\ dt = \int \varphi\ \Delta T(t)\ dt \quad (6)$$

The middle term corresponds to the reversible path and the right-hand term is the path taken during the experiment. The latter expression is the integral form of Eq. 5 with f = 0 (no more electric field applied).

Eq. 6 is only valid if the initial and final states are the same using both paths. It is likely that for a final temperature in the middle of the phase transition the two paths are not equivalent since the phase transition dynamic depends on the cooling rate. Consequently, values of energy and entropy in the mixed phase state should be regarded with caution.

Using the aforementioned δQ_{rev} profile, we can express the entropy variation with Eq. 7.

$$dS = \frac{\delta Q_{rev}}{T_{rev}} \approx \frac{\delta Q_{rev}}{T_{env}} \quad (7)$$

T_{rev} is the hypothetical temperature profile followed during the reversible path. If the temperature variations are small compared to the initial temperature, the temperature profile in the denominator can be approximated by its average value. As we are working near room temperature, we simply approximate T_{rev} by T_{env}.

Combining Eqs. 6 and 7 we obtain an expression for the total entropy variation as the sample cools down through the phase transition.

$$\Delta S \approx \frac{\varphi}{T_{env}} \int \Delta T(t) dt \quad (8)$$

Equation 8 gives us the entropy variation the sample undergoes during cooling using the experimentally measured profile $\Delta T(t)$. If the phase transition is fully crossed it gives the associated change in entropy and away from this transition the heat capacity of the material can be obtained.

5. Measurement and discussion

We applied this principle to an 83 mg bulk PST sample. PST is known to exhibit a ferroelectric to paraelectric phase transition near room temperature. This transition is particularly sharp for high degree of order PST arrangements [19]. The order parameter corresponding to the bulk PST is equal to 0.96 and it has been deduces using integrated areas of the 111 supercell and 200 unit cell diffraction peaks with X-ray diffraction (XRD) characterization method (Figure in supplementary). Details of characterization method and calculation of the order parameter can be found in materials and methods section. The microstructure quality was assessed using the scanning electron microscopy (SEM) as described in materials and methods section. The average grain size is 2.4 micrometres. Pores are in average 0.9 microns in diameter and the surface density is one pore per 126 μm^2 (figure in supplementary).

The stage temperature was initially set to 10 °C, slightly lower than the expected Curie temperature of the sample; the surface temperature was measured at 10.8 °C. The dimensions were 0.2 cm^2 for surface area, 0.5 mm for thickness. With a thermal conductivity measured at 1 $Wm^{-1}K^{-1}$ the Biot number is 5.10^{-4}. This confirmed that we could consider a homogeneous temperature inside the sample.

A first measurement of temperature was performed at 100 Hz to extract φ. When the steady state is reached, the dielectric and ferroelectric losses exactly compensate for the power dissipated in the sample and both A and ΔT are constant. In this case, Eq. 5 can be rewritten as Eq. 9.

$$\frac{Af}{\Delta T} = -\varphi \quad (9)$$

In principle, it is not necessary to measure φ with a first experiment before measuring the phase transition. This is because Eq. (8) and (9) can be used on the same temperature curve. However, getting the value of φ with Eq. 9 requires measuring accurately the polarization losses in the sample, which is easier to do when the sample remains ferroelectric throughout the experiment. Indeed, the Sawyer-Tower not only captures the polarization but also extrinsic contributions coming from the circuit parasitic resistance. In the ferroelectric state, the circuit losses are still present, but the area of the hysteresis curve is predominantly due to the ferroelectric loses. In that case, we can be certain that the energy is dissipated inside the sample and not elsewhere.

At the chosen frequency of 100 Hz the sample heated up but stayed in the ferroelectric phase. The polarization was measured in-situ once the steady state was reached, yielding a coefficient φ equal to 25 mW K^{-1} kg^{-1}. The measurement was then performed with higher frequency and voltage to heat up the sample above the ferroelectric-paraelectric transition. The polarization was not recorded any longer

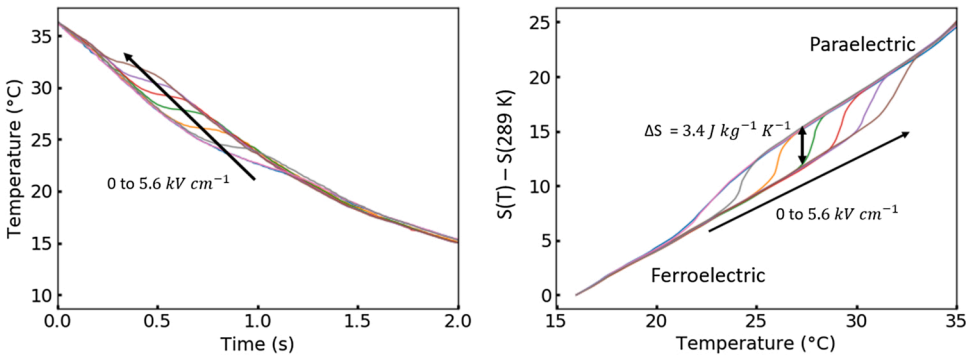

Fig. 3. – a) Temperature profiles observed with the IR camera on PST after the latter has been self-heated. Each curve corresponds to a different electric field bias, ranging from 0 to 5.6 kV cm^{-1}. All profiles were collected while temperature was decreasing and b) entropy variation obtained from the temperature profiles and Eq. 8.

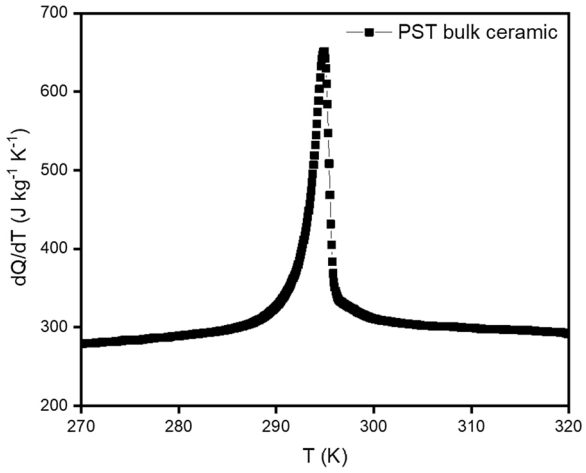

Fig. 4. Heat capacity of PST upon cooling measured with a differential scanning calorimeter.

as the coefficient of heat exchange φ was previously determined.

This was repeated several times but this time with a DC bias, applied right after the AC signal cut-off, as the sample started cooling. As mentioned previously this bias does not impact significantly the entropy calculation, provided the Joule effect is negligible. The measured temperature profiles are displayed in Fig. 3a while Fig. 3b shows the resulting entropy diagram, deduced from Eq. 8.

Applying a 700 Hz-signal, a steady state was reached within the sample at 36 °C. At t = 0 the AC field is removed and instantaneously replaced by a DC bias. Upon cooling down the sample crosses the Curie temperature and transits back to the ferroelectric state. Since PST has a first order phase transition, latent heat is released. This creates a disruption in the temperature profile, with the visible appearance of a bump (cf Fig. 3). Fig. 3.a is a zoom-in on the area of interest for the latent heat measurement, an example of complete temperature profile is shown is supplementary Section 2.

The entropy variation is calculated from this temperature profile $\Delta T(t)$ and Eq. 8. The entropy is arbitrarily set in reference to that at 16 °C, away from the transition. In the entropy-temperature (S-T) diagram, the phase transition is visible as a jump from an upper to a lower branch. The DC biases applied to the sample correspond to electric fields values ranging from 0 to 5.6 kV cm^{-1}. The electric field shifts linearly the Curie temperature to higher values as seen by the shift of the bumps and jumps (Fig. 3a and b). The presence of several curves at different biases makes obvious the entropy branches of the ferroelectric and paraelectric phases and the jump in between. Here an entropy change of 3.4 J kg^{-1}K^{-1} is measured. The slope of the entropy diagrams out of the 'jumping zone' also yields the background heat capacity of the material (here 290 J kg^{-1}K^{-1}). As a point of comparison, we measured these quantities using DSC, the resulting scan is shown in Fig. 4.

In Fig. 4, the total entropy change associated with the phase transition is obtained by integrating the peak area. To get a proper value of the integral, the baseline is interpolated, and then subtracted to the signal. This measurement gave an entropy change of 3.36 J kg^{-1}K^{-1} upon heating and 3.64 J kg^{-1}K^{-1} upon cooling. This is in agreement with the measurement presented in this article as well as values from the literature on similarly ordered samples [17,21].

The main interest of this method is that it requires the same equipment as that of the adiabatic temperature change characterization. When applicable, this makes the characterization of the electrocaloric effect quite complete with a measurement of both ΔT and ΔS. It is also significantly faster than DSC, e.g the set of curves in Fig. 3 was obtained in under fifteen minutes.

6. Limitations and ways of improvement

An experimental change that is neither a limitation nor a benefit: the dimension requirements. With this approach it is possible to measure larger samples that is possible using DSC. Indeed, the studied sample weights 83 mg, when commercial calorimeters typically require samples below 30 mg. On the other hand, the sample must be flat and thin enough so that the Biot number remains small.

For polarization measurements we used a Sawyer-Tower circuit. This has the advantage of using the same setup as the one used for heating. However, it is not very accurate compared to virtual ground circuits. In the paraelectric phase in particular, the presence of parasitic losses in the circuit can be significant compared to intrinsic material losses. Any error on the hysteresis directly impacts the evaluation of φ (Eq. 9) and calculated entropy.

Regarding temperature measurements, we used an infrared camera with a temperature resolution of 20 mK, which is enough for the variations involved. However, this requires the use of black paint, which adds some inert thermal mass on the top of the sample. Its thickness, measured with a profilometer, is in the 10−20 μm range. This is small enough to be disregarded but it does add up as a source of error. Other tools such as thermocouples could be used just as efficiently as IR camera, provided they are accurate, small and fast enough.

Aside from the standard precision issues mentioned above, there are two main limitations to this method. First, the range of applications needs to be extended. Cooling technologies are typically working in the -20 °C + 50 °C range and a characterization method should at least cover that range. The assumptions on heat exchange made throughout this work would most likely not work on a material whose Curie temperature is at 50 °C. A temperature-controlled enclosure is needed to maintain the sample in the same conditions as those presented here. This is difficult to

do while using an infrared camera and thermocouples might be easier to use in that case.

Secondly, we only obtain the cooling part of latent heat with this approach and thus lack information on the thermal hysteresis of the material. It should be possible to obtain it but would require recording the polarization throughout heating. Calculating the entropy would then require a good control of the parasitic losses in the circuit because a simple measurement of σ_c as we did would not be sufficient.

7. Conclusion

Polarization losses in ferroelectric and dielectric materials provide a simple way to heat up a sample in a controlled fashion. By taking advantage of this, we presented a method to measure the entropy change ΔS associated to the first order phase transition of lead scandium tantalate. The set-up used is the same as the one required for the measurement of adiabatic temperature change ΔT, making it possible to obtain simultaneously the two main figures of merit ΔT and ΔS of an electrocaloric material. We applied this principle to highly ordered bulk ceramic PST and obtained an entropy change of 3.4 J $kg^{-1}K^{-1}$. As it is also much faster than standard calorimetry, this method could prove useful for large electrocaloric characterization campaigns. This method should prove of interest in the study of electrocaloric materials whose performances are optimal near phase transitions.

Declaration of Competing Interest

We declare that this manuscript is original, has not been published before and is not currently being considered for publication elsewhere. The authors declare no competing interests.

Acknowledgements

P.L., A.T., Y.N. and E.D. acknowledge the Fonds National de la Recherche (FNR) of Luxembourg for supporting this work through the projects CAMELHEAT C17/MS/11703691 and MASSENA PRIDE/15/10935404.

Appendix A. Supplementary data

Supplementary material related to this article can be found, in the online version, at doi:https://doi.org/10.1016/j.jeurceramsoc.2021.07.002.

References

[1] X. Moya, S. Kar-Narayan, N.D. Mathur, Caloric materials near ferroic phase transitions, Nat. Mater. 13 (5) (2014) 439–450, https://doi.org/10.1038/nmat3951.

[2] G. Zhang, Q. Li, H. Gu, S. Jiang, K. Han, M.R. Gadinski, M.A. Haque, Q. Zhang, Q. Wang, Ferroelectric polymer nanocomposites for room-temperature electrocaloric refrigeration, Adv. Mater. 27 (8) (2015) 1450–1454, https://doi.org/10.1002/adma.201404591.

[3] D. Sette, A. Asseman, M. Gérard, H. Strozyk, R. Faye, E. Defay, Electrocaloric cooler combining ceramic multi-layer capacitors and fluid, APL Mater. 4 (9) (2016) 091101, https://doi.org/10.1063/1.4961954.

[4] X.-S. Qian, H.-J. Ye, Y.-T. Zhang, H. Gu, X. Li, C.A. Randall, Q.M. Zhang, Electrocaloric materials: giant electrocaloric response over a broad temperature range in modified BaTiO3Ceramics (Adv. Funct. Mater. 9/2014), Adv. Funct. Mater. 24 (9) (2014) 1336, https://doi.org/10.1002/adfm.201470060.

[5] C.S. Alves, S. Gama, A. Coelho, A. de, E.J.R. Plaza, A.M.G. Carvalho, L.P. Cardoso, A.C. Persiano, Giant magnetocaloric effect in Gd5(Si2Ge2) alloy with low purity Gd, Mater. Res. 7 (4) (2004) 535–538, https://doi.org/10.1590/S1516-14392004000400005.

[6] S. Kar-Narayan, S. Crossley, X. Moya, V. Kovacova, J. Abergel, A. Bontempi, N. Baier, E. Defay, N.D. Mathur, Direct electrocaloric measurements of a multilayer capacitor using scanning thermal microscopy and infra-red imaging, Appl. Phys. Lett. 102 (3) (2013) 032903, https://doi.org/10.1063/1.4788924.

[7] M.P. Annaorazov, S.A. Nikitin, A.L. Tyurin, K.A. Asatryan, A.K. Dovletov, Anomalously high entropy change in FeRh alloy, J. Appl. Phys. 79 (3) (1996) 1689–1695.

[8] C. Zhili, N. Setter, L.E. Cross, Diffuse ferroelectric phase transition and cation order in the solid solution system Pb(Sc1/2Nb1/2)O3:Pb(Sc1/2Ta1/2)O3, Ferroelectrics 37 (1) (1981) 619–622, https://doi.org/10.1080/00150198108223500.

[9] X. Moya, E. Stern-Taulats, S. Crossley, D. González-Alonso, S. Kar-Narayan, A. Planes, L. Mañosa, N.D. Mathur, Giant electrocaloric strength in single-crystal BaTiO3, Adv. Mater. 25 (9) (2013) 1360–1365, https://doi.org/10.1002/adma.201203823.

[10] W. Geng, Y. Liu, X. Meng, L. Bellaiche, J.F. Scott, B. Dkhil, A. Jiang, Giant negative electrocaloric effect in Antiferroelectric La-Doped Pb(ZrTi)O3Thin films near room temperature, Adv. Mater. 27 (20) (2015) 3165–3169, https://doi.org/10.1002/adma.201501100.

[11] P. Vales-Castro, R. Faye, M. Vellvehi, Y. Nouchokgwe, X. Perpinà, J.M. Caicedo, X. Jordà, K. Roleder, D. Kajewski, A. Perez-Tomas, E. Defay, G. Catalan, Origin of the large negative electrocaloric effect in antiferroelectric PbZrO3. ArXiv: 2009.02184 [Cond-Mat], 2020. https://arxiv.org/abs/2009.02184.

[12] K.K. Nielsen, H.N. Bez, L. von Moos, R. Bjørk, D. Eriksen, C.R.H. Bahl, Direct measurements of the magnetic entropy change, Rev. Sci. Instrum. 86 (10) (2015) 103903, https://doi.org/10.1063/1.4932308.

[13] G. Sebald, L. Seveyrat, J.-F. Capsal, P.-J. Cottinet, D. Guyomar, Differential scanning calorimeter and infrared imaging for electrocaloric characterization of poly(vinylidene fluoride-trifluoroethylene-chlorofluoroethylene) terpolymer, Appl. Phys. Lett. 101 (2) (2012) 022907, https://doi.org/10.1063/1.4734924.

[14] V. Basso, F. Russo, J.-F. Gerard, S. Pruvost, Direct measurement of the electrocaloric effect in poly(vinylidene fluoride-trifluoroethylene-chlorotrifluoroethylene) terpolymer films, Appl. Phys. Lett. 103 (20) (2013) 202904, https://doi.org/10.1063/1.4830369.

[15] J. Zheng, S. Takahashi, S. Yoshikawa, K. Uchino, J.W.C. de Vries, Heat generation in multilayer piezoelectric actuators, J. Am. Ceram. Soc. 79 (12) (1996) 3193–3198, https://doi.org/10.1111/j.1151-2916.1996.tb08095.x.

[16] O. Malyshkina, A. Eliseev, R. Grechishkin, Heat losses in ferroelectric ceramics due to switching processes, Proc. Est. Acad. Sci. 66 (4) (2017) 462, https://doi.org/10.3176/proc.2017.4.07.

[17] B. Nair, T. Usui, S. Crossley, S. Kurdi, G.G. Guzmán-Verri, X. Moya, S. Hirose, N. D. Mathur, Large electrocaloric effects in oxide multilayer capacitors over a wide temperature range, Nature 575 (7783) (2019) 468–472, https://doi.org/10.1038/s41586-019-1634-0.

[18] A. Torelló, P. Lheritier, T. Usui, Y. Nouchokgwe, M. Gérard, O. Bouton, S. Hirose, E. Defay, Giant temperature span in electrocaloric regenerator, Science 370 (6512) (2020) 125–129, https://doi.org/10.1126/science.abb8045.

[19] W. Dmowski, M.A. Akbas, P.K. Davies, T. Egami, Local structure of Pb (Sc1/2 Ta1/2) O3 and related compounds, J. Phys. Chem. Solids 61 (229) (2000).

[20] X.X.H.-Ch. Wang, W.A. Schulze, Order-disorder phenomenon in lead scandium tantalite, J. Am. Ceram. Soc. 73 (5) (1990) 1228–1234.

[21] Y. Nouchokgwe, P. Lheritier, C.H. Hong, R.Faye A.Torello, W. Jo, C. Bahl, E. Defay, Giant electrocaloric materials energy efficiency in highly ordered lead scandium tantalate, Nat. Commun. (2021).